Modelling of Shear-Driven Liquid Wall Films on Curved Surfaces: Effect of Accelerated Air Flow and Variable Film Load

J. Ebner, P. Schober, O. Schäfer, S. Wittig

Lehrstuhl und Institut für Thermische Strömungsmaschinen (ITS)
Universität Karlsruhe (TH)
76128 Karlsruhe, Germany

Liquid wall films that are driven by the shear stress exerted from a co-current air stream occur in many technical systems, e.g. in rocket nozzles, heat exchangers and on steam turbine blades. They are also present in prefilming airblast atomisers which are used for the fuel preparation in modern aviation gas turbines. In many cases an acceleration of the co-current air flow is imposed either in order to improve the performance or because of the geometrical constraints in complex configurations. Additionally, the film load Λ_f (volume flow rate per unit width) varies as a consequence of the contour of the flow passage, e.g. in concentric nozzles. The film flow characteristics are strongly influenced by both effects which will be discussed in detail.
In order to predict the two-phase flow field, a model has been developed which allows a fully coupled computation of the gas flow field and the liquid film. The present paper highlights the main features of the model which allow to capture the effect of the imposed pressure gradient dP/dx and the varying film load Λ_f at the same time. It will be shown that the numerical approach is capable to predict the film propagation with a high accuracy, providing a powerful tool for the design and the improvement of technical applications where liquid film phenomena play an important role.

1. Nomenclature

Latin symbols

A^+	$-$	constant in wall function
b	m	width of liquid film
c	$-$	mass concentration
$\vec{c}$	m/s	velocity vector $\vec{c} = (u,v,w)$
c_f	$-$	friction coefficient
c_p	$J/(kg\,K)$	specific heat
h	J/kg	enthalpy of evaporation
h_f	m	mean film thickness
H	m	height
H	J	enthalpy
$\dot{H}''$	W/m^2	enthalpy flux
J	$(kg\,m)/s$	momentum
k_s	m	equiv. sand grain roughness
$\dot{m}$	kg/s	mass flow rate
On_f	$-$	Ohnesorge number $On_f = \sqrt{\nu_f^2 \rho_f / (\sigma_f h_f)}$
p^+	$-$	non-dimen. pressure gradient $p^+ = \nu \sqrt{\rho/\tau_{f,s}^3}\, dP/dx$
P	Pa	pressure
$\dot{Q}''$	W/m^2	heat flux
R	m	radius
S	var.	source term
T	K	temperature
u,v,w	m/s	velocity in x,y,z-direction
u_τ	m/s	shear velocity $u_\tau = \sqrt{\tau_{f,s}/\rho_g}$
We_f	$-$	Weber number $We_f = \tau_{f,m}\, h_f/\sigma_f$
x,r,φ	$m,m,^\circ$	cylindrical coordinates
x,y,z	m,m,m	cartesian coordinates

Greek symbols

α	$^\circ$	flow angle of the streamline close to the wall
α	$W/(m^2 K)$	conv. heat transfer coefficient
δy_0^+	$-$	constant in wall function
ε_t	m^2/s	eddy viscosity
λ	$W/(m\,K)$	thermal conductivity
ν	m^2/s	kinematic viscosity
ρ	kg/m^3	density
τ	N/m^2	shear stress
σ	N/m	surface tension

Γ	var.	effective diffusion coefficient	*out*	outlet
Λ_f	m^2/s	film load $\Lambda_f = \dot{m}_f/(\rho_f b)$	*s*	surface
Φ	var.	transport variable	*t*	turbulent
Ψ	–	shape factor (film roughness)	*vap*	vapour
Subscripts			*w*	wall
d		droplet	***Superscripts***	
f		film	$+$	"wall units", quantity normalised by velocity scale u_τ
g		gas		
in		inlet	$\cdot$	indicating flow rate
m		mean	$''$	normalised per unit area

2. Introduction

Shear-driven liquid wall films are present in many technical applications. They play a major role in the fuel preparation process of modern gas turbine combustors if liquid fuel is used. **Fig. 1(a)** shows the design of a prefilming airblast atomiser commonly used to create a fine fuel spray. The liquid is typically supplied by a pressure nozzle. The droplets hit the wall and a film is formed which is then driven by shear forces imposed by the co-current gas flow to the atomiser lip. There, the liquid film is disintegrated into small droplets by the aerodynamic forces from the inner and outer swirling air flow. Obviously, the velocity of the co-current air flow and thus the driving shear forces of the film vary along the flow path. In more advanced atomiser designs, a distinctive acceleration of the air flow is used to manipulate the liquid film propagation, e.g. by applying a concentric nozzle.

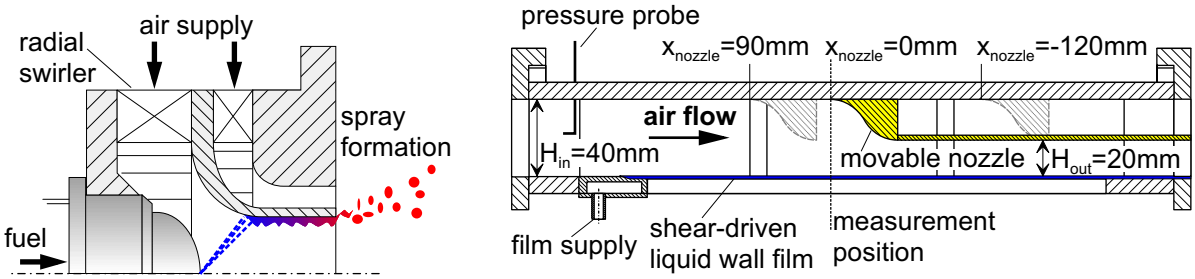

(a) Sketch of atomiser **(b)** Test section for plane film flow experiments

Fig. 1 Generic prefilming airblast atomiser and rectangular duct for plane film flow investigations

In order to predict the film flow propagation in such a flow configuration, enhanced models have to be developed, which take into account the pressure gradient of the air flow and the variation of the film load Λ_f as consequence of the contour of the flow passage. In the present paper an improved model for predicting the two-phase flow field in any nozzle geometry is presented. The numerical results are compared to measurements in a rectangular test section as depicted in **Fig. 1(b)** and a concentric nozzle to capture the different physical effects. In the first case plane film flows will be discussed with only a pressure gradient dP/dx present, whereas in the second case also a strong increase of the film load Λ_f can be observed. The inclusion of the effect of the pressure gradient on the momentum transfer at the gas-liquid interface has already been presented elsewhere [1].

3. Coupled two-phase flow prediction

In order to predict the complex two-phase flow field by a numerical approach, a fully coupled treatment of the gas flow and the liquid wall film is required. The CFD-code developed consists of the following components. The turbulent air flow is predicted by the ITS in-house 3d Navier Stokes code METIS for body-fitted grids and with the standard k-ε-turbulence model [2]. The wall

functions of the gas solver have been extended to take into account the effect of roughness in the momentum, heat and mass transfer to the wall. The liquid wall film is calculated by the external module PROFILM utilising a 2d boundary layer approach. Thereby, the liquid film is modelled as a turbulent boundary layer flow and the governing equations are solved by a finite difference method.

The main exchange parameters for momentum, heat and mass are the equivalent sand grain roughness k_s, the surface temperature $T_{f,s}$ and the evaporated mass flux $\dot{m}''_{vap}$ predicted by the film module. The gas solver provides the shear stress at the gas-liquid interface $\tau_{f,s}$, the gas temperature T_g and the vapour mass concentration c_{vap}. The momentum transfer from the co-current air flow to the liquid wall film, for example, is realised by the following procedure. The roughness of the film surface is assigned to the gas solver by the equivalent sand grain roughness k_s which depends on the film thickness h_f and a special shape factor Ψ accounting for the exact structure of the film surface (see **Eq. 3**). After taking into account the roughness of the wall, the shear stress $\tau_{f,s}$ along the wall is predicted by the gas solver and provided to the film module for the next iteration step. For a more detailed overview of the major features and the coupling of the gas solver METIS and the film module PROFILM the reader is referred to [1].

4. Gas flow solver

As mentioned before, the turbulent gas flow field is calculated with the in-house code METIS. The code is based on a finite volume method. Various discretisation schemes (UPWIND, MLU) are available. The Reynolds-averaged equations for the momentum, heat and mass transfer can be expressed as

$$div\left(\rho\,\vec{c}\,\Phi\right) = div\left(\Gamma_\Phi \cdot grad\Phi\right) + S_\Phi \tag{1}$$

where Γ_Φ is an effective diffusion coefficient and S_Φ denotes the source term of the transport variable Φ. Details on the mathematical solution are given in [3, 4].

Commonly, the logarithmic wall function is used for the closure of the gas flow equations at solid walls in turbulent air flow [2]. The roughness of the wall as well as the pressure gradient in the air flow are usually neglected. Whereas the impact on the overall air flow field is rather small, the prediction of the interfacial parameters to a rough wall is poor. In order to predict the air flow above wavy films in nozzles and diffusors a modified boundary layer approach based on the assumption of van Driest is applied, introducing a damping function for the viscous sublayer according to Kays and Crawford [5–7]. The eddy viscosity ε_t reads

$$\frac{\varepsilon_t}{\nu} = \kappa^2 \left(y^+ + \delta y_0^+\right)^2 \left(1 - e^{-y^+/A^+}\right)^2 \left|\frac{\partial u^+}{\partial y^+}\right| \tag{2}$$

with the damping function $D = (1 - \exp(-y^+/A^+))$. The parameters A^+ in the damping function D and δy_0^+ for fully rough walls allow a detailed description of the transition from the turbulent region of the boundary layer to the viscous sublayer. The effects of the wall roughness k_s and the pressure gradient dP/dx on the boundary layer are taken into account simultaneously [8].

In order to capture the roughness effect of the liquid wall film, the equivalent sand grain roughness k_s has to be determined from film flow parameters. Following a suggestion of Wurz [9] the waviness of the film can be reflected by the equivalent sand grain roughness as indicated in **Fig. 2(a)**. The sand grain roughness is simply related to the film thickness h_f by

$$k_s = 2 \cdot h_f \cdot \Psi\left(We_f, On_f, \sigma_f, p^+\right) \tag{3}$$

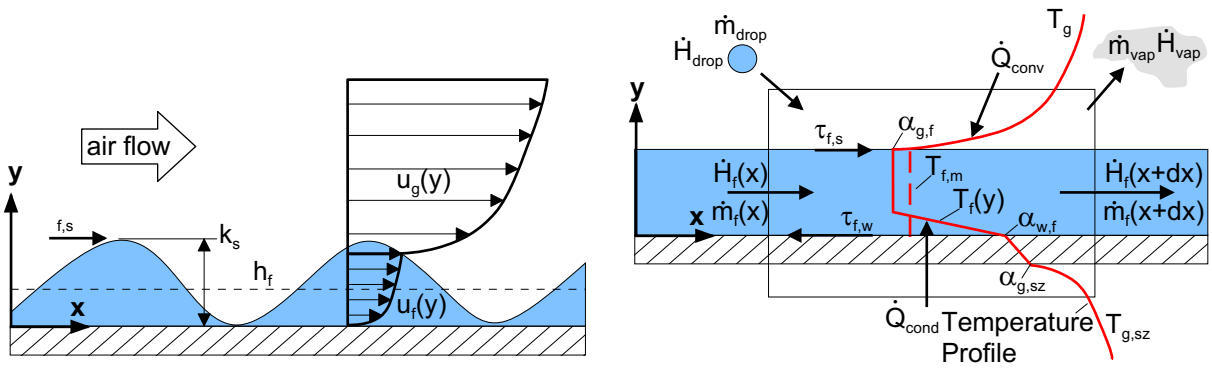

(a) Simplified model for roughness **(b)** Mass and enthalpy balance scheme

Fig. 2 Model for shear-driven liquid wall films

where Ψ is the shape factor which takes into account the surface structure of the wall film. It has been shown by Ebner et al. [1] that this parameter strongly depends on the liquid properties and the film flow conditions.

5. Model for liquid film flow

Based on the boundary layer equations [10], the conservation of mass, momentum and heat can be deduced from a balance at the control volume displayed in **Fig. 2(b)**. The following set of equations can be formulated for the calculation of liquid wall film flows.

Conservation of mass:

$$\frac{\partial \dot{m}_f}{\partial x} = \frac{\partial}{\partial x} \int_0^{b(x)} \int_0^{h_f(x)} \rho_f \, u_f(x,y) \, dy\, dz = \left[-\dot{m}''_{vap} + \dot{m}''_d \right] \cdot b \tag{4}$$

Conservation of momentum:

$$\frac{\partial \dot{J}_f}{\partial x} = \frac{\partial}{\partial x} \int_0^{b(x)} \int_0^{h_f(x)} \rho_f \, u_f^2(x,y) \, dy\, dz = \left[(\tau_{f,s} - \tau_{f,w}) - \frac{dP}{dx} h_f - \dot{m}''_{vap} \, u_{f,s} + \dot{m}''_d \, u_d \right] \cdot b \tag{5}$$

Conservation of enthalpy:

$$\frac{\partial \dot{H}_f}{\partial x} = \frac{\partial}{\partial x} \int_0^{b(x)} \int_0^{h_f(x)} \rho_f \, c_{p,f} \, u_f(x,y) \, T_f(x,y) \, dy\, dz = \left[\dot{Q}''_{cond} + \dot{Q}''_{conv} - \dot{H}''_{vap} + \dot{H}''_d \right] \cdot b \tag{6}$$

Several assumptions on the momentum and heat exchange within the film are required to derive differential equations which can then be evaluated numerically. The experimental work of Elsäßer [11] revealed that the momentum flux of shear-driven liquid wall films is represented very well utilising a block profile for the internal film velocity distribution $u_f(x,y)$. On the other hand a turbulent boundary layer approach according to Wurz [12] can be applied to describe the velocity profile close to the wall in order to determine the wall shear stress $\tau_{f,w}$. Therefore, the hybrid model presented in this paper consists of a block profile for the film velocity $u_f(x,y) = u_{f,m}(x)$ in the conservation equations and a fully turbulent approach for the computation of the shear stress $\tau_{f,w}$ at the wall in **Eq. 5**.

Based on the conservation equations for mass, momentum and enthalpy and utilising the definition of the film load Λ_f and the mass averaged mean film temperature $T_{f,m}$ according to

$$\Lambda_f = \int_0^{h_f(x)} u_f(x,y)\,dy = u_{f,m}\cdot h_f \quad \text{and} \quad T_{f,m} = \frac{\int_0^{h_f(x)} u_f(x,y)\cdot T_f(x,y)\,dy}{\int_0^{h_f(x)} u_f(x,y)\,dy} \tag{7}$$

the following set of differential equations for the film load Λ_f, the mean film velocity $u_{f,m}$ and the mean film temperature $T_{f,m}$ can be deduced.

Film load:

$$\frac{\partial \Lambda_f}{\partial x} = \frac{1}{\rho_f}\left[-\dot{m}''_{vap} + \dot{m}''_d\right] - \Lambda_f \frac{1}{b}\frac{\partial b}{\partial x} \tag{8}$$

Mean film velocity:

$$\frac{\partial u_{f,m}}{\partial x} = \frac{(\tau_{f,s} - \tau_{f,w}) - \dfrac{dP}{dx} h_f + \dot{m}''_d\,(u_d - u_{f,m})}{\rho_f\,\Lambda_f} \tag{9}$$

Mean film temperature:

$$\frac{\partial T_{f,m}}{\partial x} = \frac{\dot{Q}''_{cond} + \dot{Q}''_{conv} - (\dot{H}''_{vap} - c_{p,f}\,\dot{m}''_{vap}\,T_{f,m}) + (\dot{H}''_d - c_{p,f}\,\dot{m}''_d\,T_{f,m})}{c_{p,f}\,\rho_f\,\Lambda_f} \tag{10}$$

The sources terms of the enthalpy in **Eq. 10** read

$$\begin{aligned} &\dot{Q}''_{cond} = -\lambda_f \left(\frac{\partial T_f(y)}{\partial y}\right)\bigg|_w, \qquad \dot{Q}''_{conv} = \alpha_{g,f}\left(T_g - T_{f,s}\right) \\ &\dot{H}''_{vap} = \dot{m}''_{vap}\left(h_{vap} + c_{p,f}\,T_{f,s}\right) \quad \text{and} \quad \dot{H}''_d = c_{p,d}\,\dot{m}''_d\,T_{d,m}\,. \end{aligned} \tag{11}$$

The waviness of the surface structure of shear-driven liquid films must also be accounted for in the determination of the enthalpy sources and the evaporated mass flow rate. A similar procedure as suggested by Himmelsbach et al. [13] and Roßkamp et al. [14] is applied to capture the roughness effect of the film in this context.

In the extended model presented in this paper the film width b and the pressure gradient dP/dx can vary along the flow path which is of importance for the prediction of wall film flows in nozzles and diffusor geometries. In axis-symmetric geometries the variation of the film load Λ_f is described by the term

$$\frac{1}{b}\frac{\partial b}{\partial x} = \frac{1}{r}\frac{\partial r}{\partial x} + \frac{1}{\cos(\alpha)}\frac{\partial \cos(\alpha)}{\partial x} \tag{12}$$

accounting for the change of the radius r and the angle α. The angle α of the streamline close to the wall and the projection of the symmetrical axis x on a differential surface element at the wall according to

$$\begin{aligned} \Lambda_f &= \frac{1}{\rho_f}\frac{\dot{m}_f}{b} = \frac{1}{\rho_f}\frac{\dot{m}_f}{2\pi\, r\, cos(\alpha)} \\ \text{with} \quad \cos(\alpha) &= \frac{\tau_{f,s}\big|_{x,r}}{\tau_{f,s}} \quad \text{and} \quad \vec{\tau}_{f,s}\big|_{x,r} = \begin{pmatrix} \tau_x \\ \tau_r \\ 0 \end{pmatrix}, \quad \vec{\tau}_{f,s} = \begin{pmatrix} \tau_x \\ \tau_r \\ \tau_\varphi \end{pmatrix} \end{aligned} \tag{13}$$

can be determined easily in the x, r, φ-system where the coordinates y, z are substituted by the radius r and the azimuth angle φ. In tubes with a constant radius r the angle α equals the well-known definition of the swirl angle. A finite difference method is applied to predict the liquid film in the direction of the streamline close to the wall. The mathematical formulation is based on a fifth order Runge-Kutta solver with an adaptive step control. With these methods an effective computation of the liquid wall film on any axis-symmetric curved surface is achieved.

6. Validation

In order to separate the different physical effects the validation of the film model is performed in two steps. First, the effect of a distinct pressure gradient dP/dx on a plane film flow is discussed. In a second step, the three-dimensional two-phase flow in a concentric nozzle is analysed.

6.1. Accelerated plane film flow

The impact of the modified boundary layer approach introduced in **Eq. 2** on the shear stress distribution $\tau_{f,s}$ of a plane film flow is presented in **Fig. 3(a)**. The height of the duct is reduced from $H_{in} = 40\ mm$ at the inlet to $H_{out} = 20\ mm$ downstream the nozzle according to the sketch displayed in **Fig. 1(b)**. The maximum of the shear stress is located significantly in front of the end of the nozzle. This flow characteristic is distinctively different to the one predicted by the logarithmic law of the wall where the maximum of the shear force is located at the very end of the nozzle as it depends directly on the maximum of the velocity. With higher film load Λ_f the shear stress $\tau_{f,s}$ increases due to the augmentation of the equivalent sand grain roughness k_s according to **Eq. 3**.

As a consequence of the shear stress distribution, the minimum of the film thickness h_f is expected to be found within the nozzle which is confirmed by **Fig. 3(b)**. The plots show a comparison of experimental data to the predictions using the improved film model for typical flow conditions of modern airblast atomisers. The film thickness distributions at the bottom wall of the test section have been measured using a non-intrusive optical system, a so-called Laser Focus Displacement Meter (LFDM) [15–17] with a spatial resolution of about 2 microns. The good agreement of the predictions and the measured data is obvious. In particular, the position of the minima as well as their values are determined at a high level of accuracy. The film is accelerated already in front of the nozzle because the nozzle clearly influences the air flow field upstream. While the acceleration

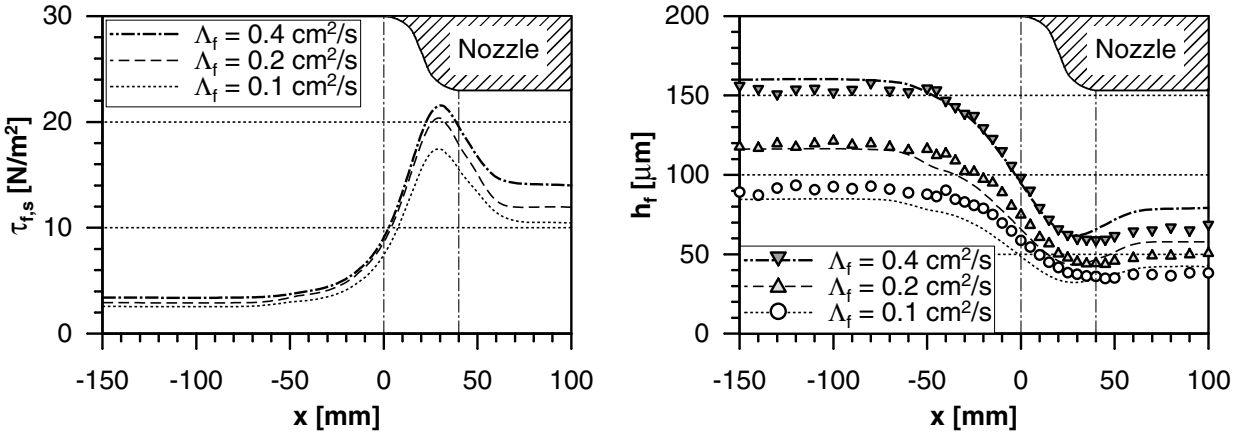

(a) Predicted shear stress distribution $\tau_{f,s}$

(b) Measured and predicted film thickness h_f (symbols: measured data, lines: prediction)

Fig. 3 Shear stress $\tau_{f,s}$ and film thickness h_f distribution in the nozzle region as function of the film load Λ_f ($P = 1\ bar$, $T = 293\ K$, $u_{g,in} = 30\ m/s$)

of the liquid film is predicted very well, minor deviations are present downstream the nozzle. This can be directly attributed to the inertia of the liquid film which is not included in the model. For that reason, the deviations increase slightly for higher film load Λ_f. In practice, this problem does not occur, as shear-driven liquid films are not decelerated abruptly in technical applications. For example, the liquid film in an airblast atomiser ends at the edge of the atomiser lip where the position of the minimum of the film thickness h_f is located.

6.2. Film flow in a concentric nozzle

In order to capture the effect of a distinct pressure gradient dP/dx and a variation of the film load Λ_f along the flow path numerical and experimental investigations have been performed for a concentric nozzle with a cone half-angle of $10°$. The radius is reduced from $R_{in} = 20\ mm$ at the inlet to $R_{out} = 11.5\ mm$ at the end of the restriction. For details about the geometry and the experimental set-up the reader is referred to Schober et al. [17].

In **Fig. 4(a)** the predicted shear stress distribution $\tau_{f,s}$ is plotted for different pressure levels. A strong increase of the interfacial forces can be observed at higher pressure P. This can be attributed to the increase of the momentum of the air flow according to

$$\tau_{f,s} = c_f \cdot \frac{\rho_g}{2} \cdot u_g^2 \tag{14}$$

where c_f is the friction coefficient of a rough wall. The friction coefficient c_f allows an alternative description of the roughness effect of wavy liquid films comparable to the procedure used in the model presented in this paper based on the shape factor Ψ defined by **Eq. 3**. According to **Eq. 13** the film load Λ_f increases from its initial value $\Lambda_{f,in} = 0.1\ cm^2/s$ to $\Lambda_{f,out}(x = 40\ mm) = 0.16\ cm^2/s$ at the end of the nozzle. Nevertheless, the film thickness h_f decreases in the nozzle which is shown in **Fig. 4(b)**. Obviously, the increase of the interfacial shear $\tau_{f,s}$ in the nozzle prevails the effect of the augmentation of the film load Λ_f. The predictions matches the experimental data well. Hence, the model can be applied to situations of high pressure.

A comparison of predicted and measured film thickness data in the nozzle as function of the air velocity u_g is presented in **Fig. 5**. The two diagrams confirm the conclusion that the film flow behaviour is controlled mainly by the momentum transfer from the co-current air flow at the gas-liquid interface. The film thickness h_f decreases with increasing air velocity u_g due to the rise of

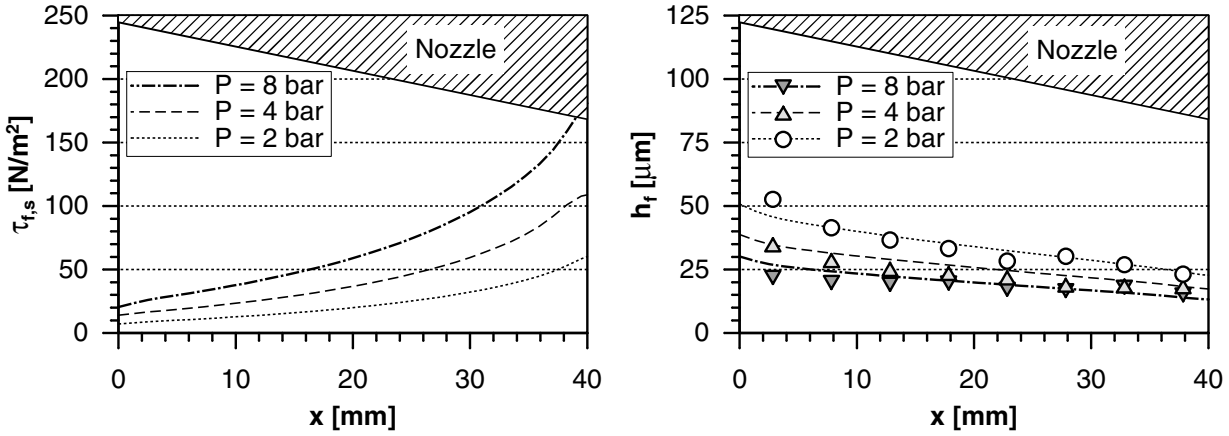

(a) Predicted shear stress distribution $\tau_{f,s}$

(b) Measured and predicted film thickness h_f (symbols: measured data, lines: prediction)

Fig. 4 Shear stress $\tau_{f,s}$ and film thickness h_f distribution as function of the pressure P in the nozzle ($\Lambda_{f,in} = 0.1\ cm^2/s$, $T = 293\ K$, $u_{g,in} = 20\ m/s$)

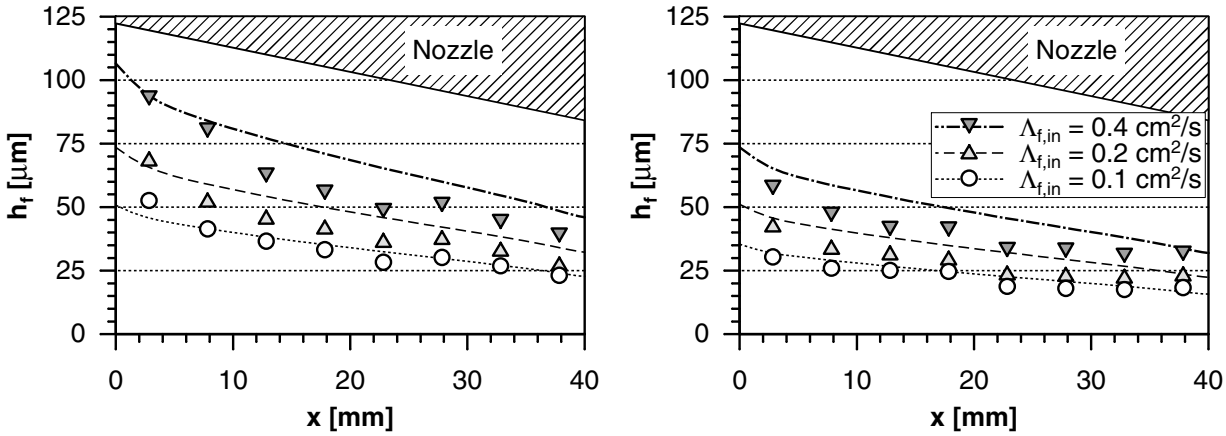

(a) Measured and predicted film thickness h_f ($P = 2\ bar$, $T = 293\ K$, $u_{g,in} = 20\ m/s$)

(b) Measured and predicted film thickness h_f ($P = 2\ bar$, $T = 293\ K$, $u_{g,in} = 30\ m/s$)

Fig. 5 Film thickness h_f distribution as function of air velocity $u_{g,in}$ at the inlet of the nozzle (symbols: measured data, lines: prediction)

the shear stress $\tau_{f,s}$ according to **Eq. 14**. The overall agreement of predicted and measured data is satisfactory.

Finally, the plots displayed in **Fig. 6** give an overview of the effect of the pressure level P on the film flow propagation at constant air velocity u_g. It is obvious, that the film thickness h_f declines at higher pressure P as already discussed before. Additionally, a comparison of **Fig. 5(b)** and **Fig. 6(a)** reveals that an augmentation of the air velocity u_g is equivalent to an increase of the pressure P. The film thickness distributions are nearly identical due to the fact that the momentum $\rho_g u_g^2$ in **Eq. 14** is almost kept constant. The increase of pressure P, and hence in the density ρ_g, is balanced by the reduction of the velocity u_g. The shape factor Ψ defined by **Eq. 3** is nearly identical in both cases because for a given film liquid it is mainly a function of the Weber number $We_f = \tau_{f,m} h_f / \sigma_f$ [1]. Thus, also the friction coefficient c_f is of the same magnitude which explains the observed results. The numerical result is also supported by the experimental findings. Schober

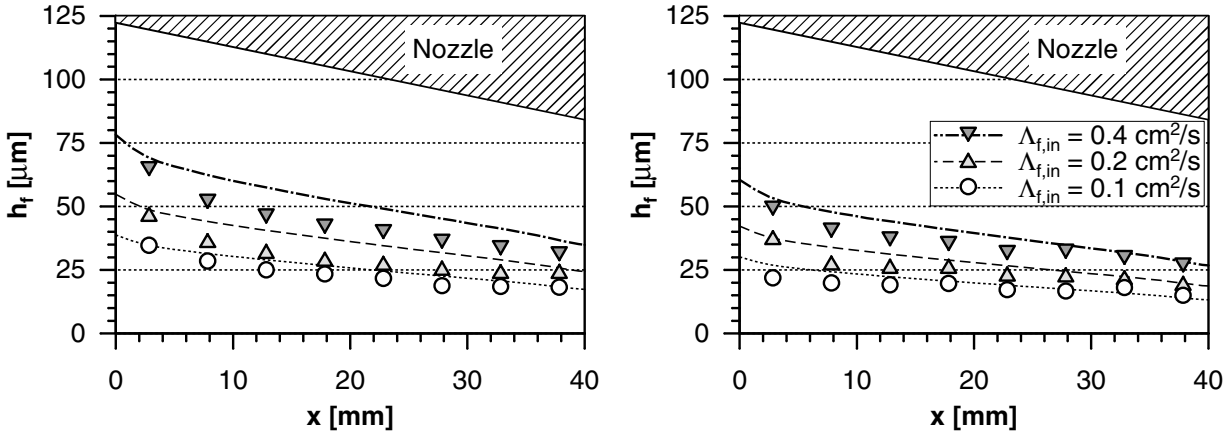

(a) Measured and predicted film thickness h_f ($P = 4\ bar$, $T = 293\ K$, $u_{g,in} = 20\ m/s$)

(b) Measured and predicted film thickness h_f ($P = 8\ bar$, $T = 293\ K$, $u_{g,in} = 20\ m/s$)

Fig. 6 Film thickness h_f distribution as function of pressure P in the nozzle (symbols: measured data, lines: prediction)

et al. [17] found that not only the film thickness distributions h_f are comparable. The visualisation of the film flow revealed that also the surface structures are almost identical in these cases which confirms the outcome of the discussion about the similarity of the two test cases.

7. Summary

Based on an improved boundary layer approach for the gaseous phase and an enhanced model for shear-driven liquid films, a numerical method has been developed by which the propagation and evaporation of liquid wall films in complex technical geometries can be predicted. In the paper the effects of an accelerated air flow and a varying film load Λ_f on the film dynamics are discussed with respect to the complex interaction at the gas-liquid interface.

The validation of the model by experimental data in a plane test section as well as in a concentric nozzle revealed that the film flow is predicted at a high level of accuracy. Thus, the method can be used for the design and optimisation of technical systems where liquid wall films play an important role. In particular, the new model is capable to handle a distinct pressure gradient dP/dx imposed by an accelerated air flow and a change of the film load Λ_f as consequence of the contour of the flow passage simultaneously.

8. Acknowledgement

This work has been supported by a grant from the 'Competitive and Sustainable Growth Programme' of the European Community under contract GRD1-1999-10325 (CFD4C) which is gratefully acknowledged.

References

[1] Ebner, J., Schober, P., Schäfer, O., Koch, R. and Wittig, S. 2003 *Modelling of Shear-Driven Liquid Wall Films: Effect of Accelerated Air Flow on the Film Flow Propagation* International Journal "Progress in Computational Fluid Dynamics" (accepted, March 2003)

[2] Launder, B. and Spalding, D. 1974 *The Numerical Computation of Turbulent Flows* Computer Methods in Applied Mechanics and Engineering **3**, pp. 269 – 289

[3] Noll, B. and Wittig, S. 1991 *Generalized Conjugate Gradient Method for the Efficient Solution of Three-Dimensional Fluid Flow Problems* Numerical Heat Transfer, Part B **20**, pp. 207 – 221

[4] Noll, B. 1992 *Evaluation of a Bounded High-Resolution Scheme for Combustor Flow Computations* AIAA Journal **30**(1), pp. 64 – 69

[5] van Driest, E. 1956 *On Turbulent Flow Near a Wall* Journal of the Aeronautical Science **8E1109/23**, pp. 1007 – 1012

[6] Kays, W. and Crawford, M. 1980 *Convective Heat and Mass Transfer* McGraw-Hill, New York

[7] Granville, P. 1985 *Mixing-Length Formulations for Turbulent Boundary Layers over Arbitrarily Rough Surfaces* Journal of Ship Research **29**(4), pp. 223 – 233

[8] Moffat, R. and Kays, W. 1984 *Advances in Heat Transfer - Review of Turbulent Boundary Layer Research* **16** Hartnett, J.P. and Irvine, T.F., Academic Press, Orlando

[9] Wurz, D. 1976 *Experimental Investigation Into the Flow Behaviour of Thin Water Films; Effect on a Cocurrent Air Flow of Moderate to High Supersonic Velocities: Pressure Distribution at the Surface of Rigid Wavy Reference Structures* Archiwum Mechaniki Stosowaney **28**(5-6), pp. 969 – 987

[10] Schlichting, H. 1962 *Boundary layer theory* McGraw-Hill, New York

[11] Elsäßer, A. 1998 *Fuel Preparation of Internal Combustion Engines: Fundamentals of the Flow of Shear-Driven Liquid Films (in german)* Phd thesis Department of Thermal Turbomachinery, University Karlsruhe, Germany

[12] Wurz, D. 1971 *Experimental Investigation of the Flow Behaviour of Thin Water Films and their Effect on a Co-current Air Flow of Moderate to High Subsonic Velocities (in german)* Phd thesis Department of Thermal Turbomachinery, University Karlsruhe, Germany

[13] Himmelsbach, J., Noll, B. and Wittig, S. 1994 *Experimental and Numerical Studies of Evaporating Wavy Fuel Films in Turbulent Air Flows* International Journal of Heat and Mass Transfer **37**, pp. 1217 – 1226

[14] Roßkamp, H., Elsäßer, A., Samenfink, W., Meisl, J., Willmann, M. and Wittig, S. 1998 *An Enhanced Model for Predicting the Heat Transfer to Wavy Shear-driven Liquid Wall Films* 3^{rd} International Conference on Multiphase Flow, Lyon, France, June 8 – 12

[15] Takamasa, T., Tamura, S. and Kobayashi, K. 1998 *Interfacial Waves on a Film Flowing Down Plate Wall in an Entry Region Measured with Laser Focus Displacement Meters* 3^{rd} International Conference on Multiphase Flow, Lyon, France, June 8 – 12

[16] Ebner, J., Gerendás, M., Schäfer, O. and Wittig, S. 2002 *Droplet Entrainment from a Shear-driven Liquid Wall Film in Inclined Ducts – Experimental Study and Correlation Comparison* ASME–Journal of Engineering for Gas Turbines and Power **124**, pp. 874 – 880

[17] Schober, P., Ebner, J., Schäfer, O. and Wittig, S. 2003 *Experimental Study on the Effect of a Strong Negative Pressure Gradient on a Shear-driven Liquid Fuel Film* Proceedings of the Ninth International Conference on Liquid Atomization and Spray Systems (*iclass03*), Sorrento, Italy